An assessment of extra-tropical cyclone precipitation extremes over the Southern Hemisphere using ERA5

Cameron McErlich[1], Adrian J. McDonald[1], James Arthur Renwick[2], and Alex J Schuddeboom[1]

[1]University of Canterbury
[2]Victoria University of Wellington

April 29, 2023

Abstract

ERA5 reanalysis is used to examine extreme precipitation using a spatially dependent precipitation threshold applied within a cyclone compositing framework. This is used to account for regional variation in precipitation generating processes within Southern Hemisphere mid-latitude cyclones across the cyclone lifecycle. The spatial extent of extreme precipitation is limited to a smaller region around the cyclone centre compared to non-extreme precipitation, though extreme precipitation displays a good spatial correlation with non-extreme precipitation. Extreme precipitation occurs more often during the deepening phase of the cyclone before it reaches a maximum depth. Precipitation occurrence at the 90th and 98th percentiles reduces to 46% and 30% of the deepening value across the cyclone lifecycle, averaged over the composite. Precipitation fraction at the 90th and 98th percentile reduces to 80% and 60% of the deepening value. Our methodology provides a quantitative assessment of precipitation extremes both spatially and temporally, within a cyclone compositing framework.

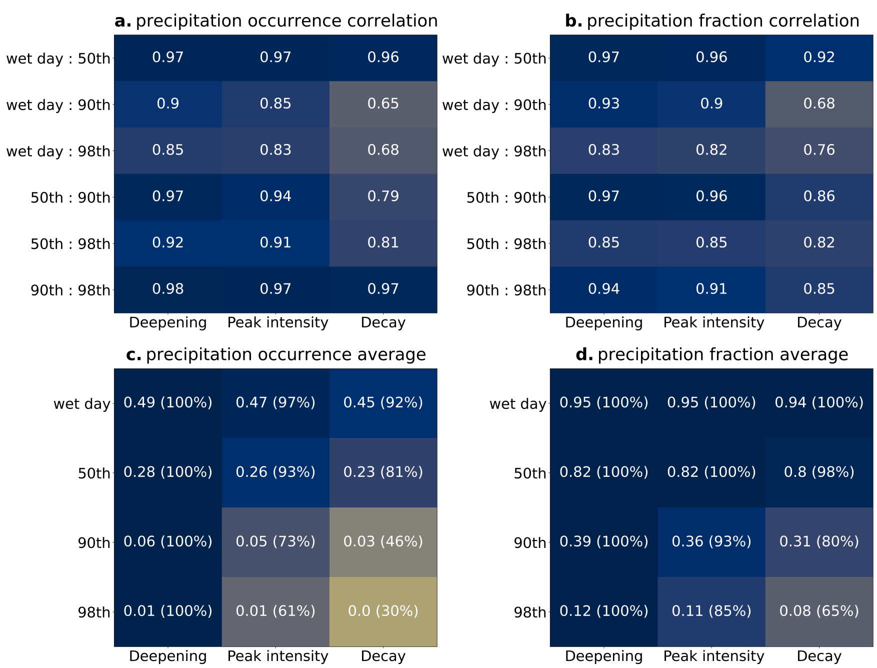

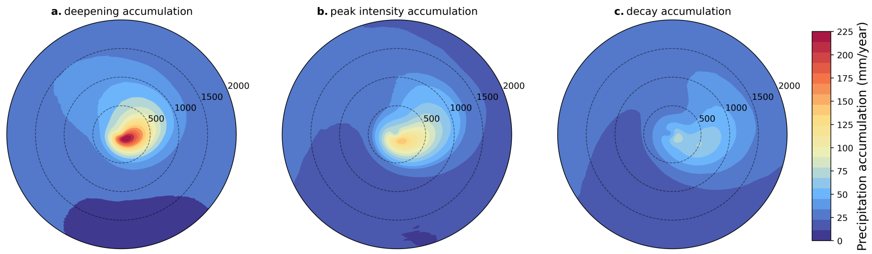
a. deepening accumulation
b. peak intensity accumulation
c. decay accumulation
500
1000
1500
2000
Precipitation accumulation (mm/year)
0
25
50
75
100
125
150
175
200
225

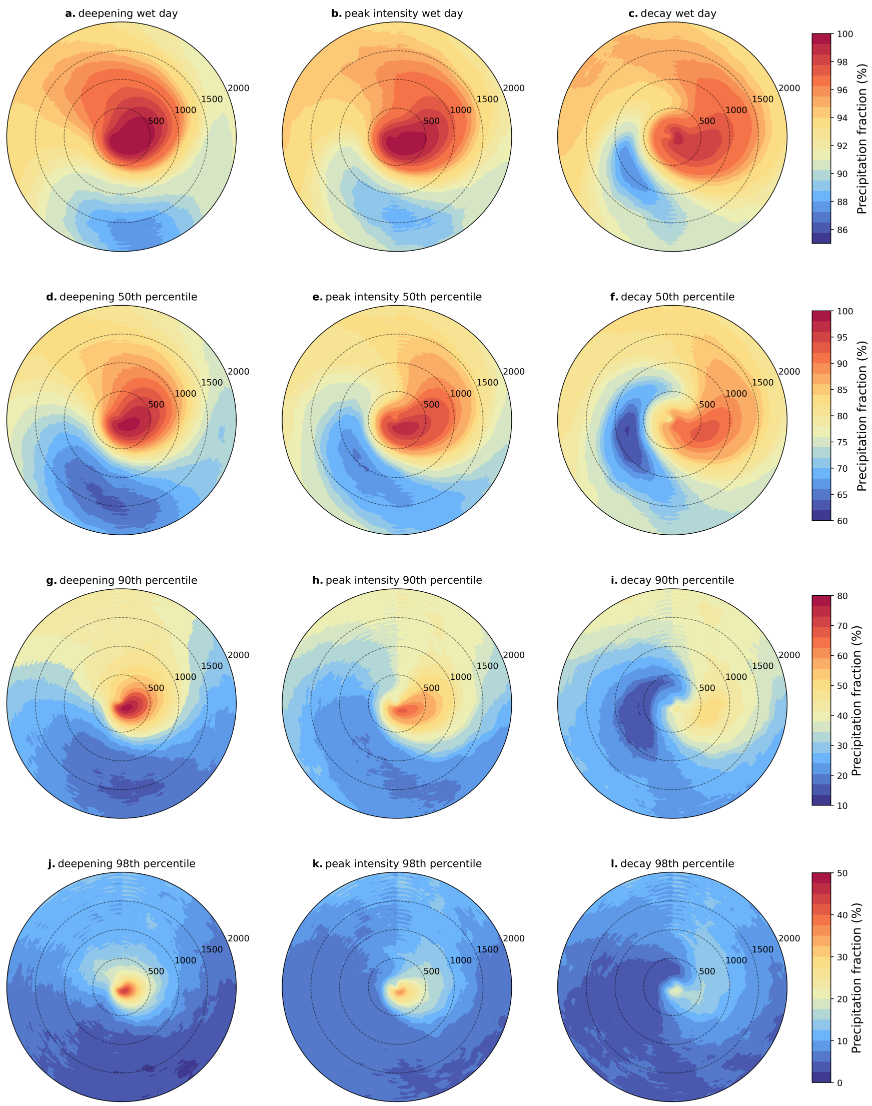
a. deepening wet day
b. peak intensity wet day
c. decay wet day
d. deepening 50th percentile
e. peak intensity 50th percentile
f. decay 50th percentile
g. deepening 90th percentile
h. peak intensity 90th percentile
i. decay 90th percentile
j. deepening 98th percentile
k. peak intensity 98th percentile
l. decay 98th percentile
500
1000
1500
2000
Precipitation fraction (%)
86
88
90
92
94
96
98
100
60
65
70
75
80
85
90
95
100
10
20
30
40
50
60
70
80
0
10
20
30
40
50

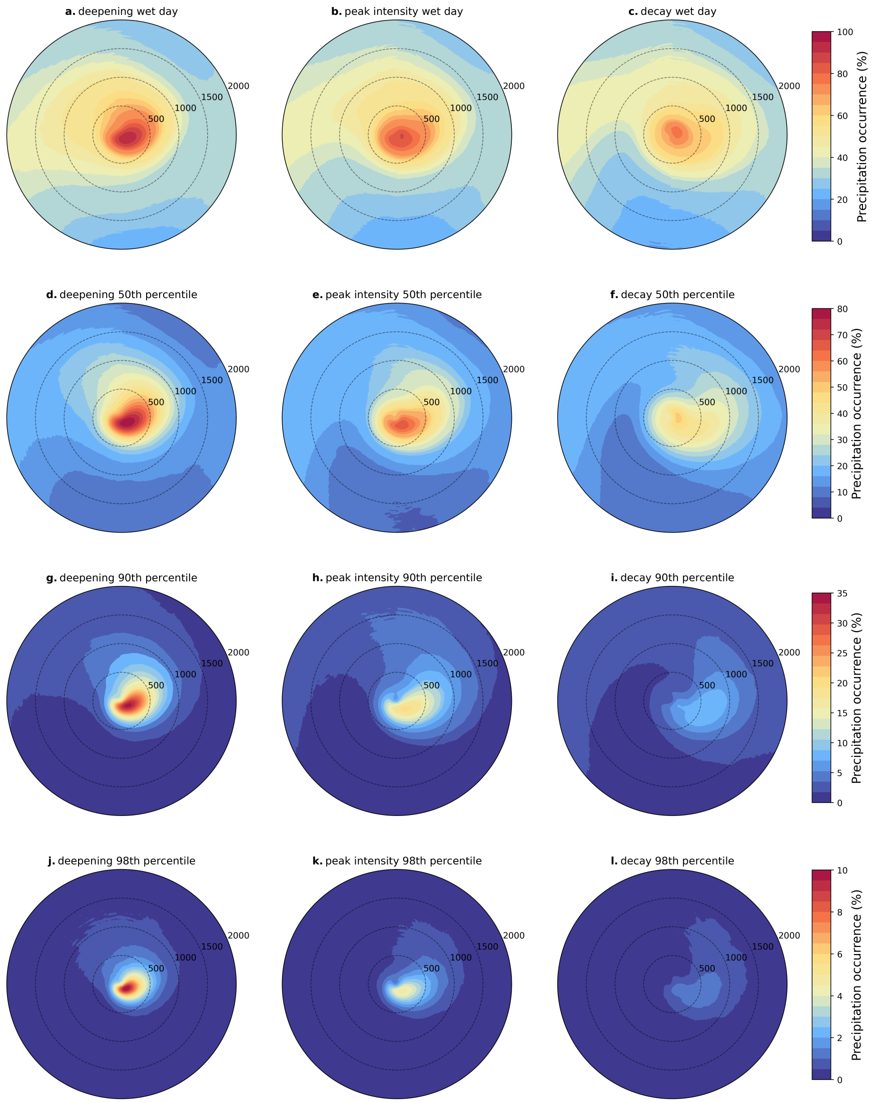
a. deepening wet day
b. peak intensity wet day
c. decay wet day
d. deepening 50th percentile
e. peak intensity 50th percentile
f. decay 50th percentile
g. deepening 90th percentile
h. peak intensity 90th percentile
i. decay 90th percentile
j. deepening 98th percentile
k. peak intensity 98th percentile
l. decay 98th percentile
500
1000
1500
2000
Precipitation occurrence (%)

An assessment of extra-tropical cyclone precipitation extremes over the Southern Hemisphere using ERA5

Cameron McErlich[1], Adrian McDonald[1,2], James Renwick[3], and Alex Schuddeboom[1]

[1]School of Physical and Chemical Sciences, University of Canterbury, Christchurch, New Zealand
[2]Gateway Antarctica, University of Canterbury, Christchurch, New Zealand
[3]Victoria University of Wellington, School of Geography, Environment and Earth Science, Wellington, New Zealand

Key Points:

- We detail a new methodology to assess precipitation extremes within cyclone composites using a spatially dependent precipitation threshold
- Extreme precipitation occurs preferentially and makes up a larger fraction of total accumulation before cyclones reach maximum depth
- As extremes increase in intensity precipitation is constrained closer to the cyclone centre and weakens more rapidly as the cyclone evolves

Corresponding author: Cameron McErlich, `cameron.mcerlich@pg.canterbury.ac.nz`

Abstract

ERA5 reanalysis is used to examine extreme precipitation using a spatially dependent precipitation threshold applied within a cyclone compositing framework. This is used to account for regional variation in precipitation generating processes within Southern Hemisphere mid-latitude cyclones across the cyclone lifecycle. The spatial extent of extreme precipitation is limited to a smaller region around the cyclone centre compared to non-extreme precipitation, though extreme precipitation displays a good spatial correlation with non-extreme precipitation. Extreme precipitation occurs more often during the deepening phase of the cyclone before it reaches a maximum depth. Precipitation occurrence at the 90th and 98th percentiles reduces to 46% and 30% of the deepening value across the cyclone lifecycle, averaged over the composite. Precipitation fraction at the 90th and 98th percentile reduces to 80% and 60% of the deepening value. Our methodology provides a quantitative assessment of precipitation extremes both spatially and temporally, within a cyclone compositing framework.

Plain Language Summary

Extra-tropical cyclones play a major role in the circulation within the atmosphere, acting to transfer heat towards the poles. Here we assess the representation of extreme precipitation within extra-tropical cyclones. By applying a threshold for precipitation that changes with geographic location, we are able to determine how extreme precipitation varies within a cyclone-centred coordinate system. When breaking cyclones into lifecycle stages representing deepening, peak intensity and decay, we find that extreme precipitation occurs most often as the cyclone is developing. The area of the cyclone relevant for extremes reduces towards the cyclone centre as the threshold for determining extreme precipitation increases. Extreme precipitation weakens at a higher rate as cyclones becomes more intense, highlighting the importance of extremes in the growth phase of the cyclone.

1 Introduction

Climate change is experienced by society through a variety of ways, including extreme weather events. Unlike long term climate trends which seem distant and occur more gradually, extremes are direct and occur in everyday life. Howe et al. (2014) suggests that people tend to accurately recall and report experiences with extreme weather, with increasing likelihood based on proximity and magnitude of an event. The impacts extremes have are numerous. Economic impacts include closure of roads, outages of power grids, water shut-offs, and physical damage to buildings, bridges, crops and livestock (Jahn, 2015). Environmental impacts include coastal erosion, changes in water supply and land coverage (Seneviratne et al., 2012; Seddon et al., 2016; Seneviratne et al., 2021). Societal impacts include food and water availability, loss of life, increasing insurance costs and changes in property values (Morss et al., 2011; Bell et al., 2018; Zscheischler et al., 2018; Konapala et al., 2020). Extreme weather has intensified in recent decades, and will continue to have a disproportionately large impact on the environment, society and the economy (Seneviratne et al., 2021).

On a global scale, precipitation extremes are predicted to increase in intensity and frequency as the climate warms (e.g. Zhang et al., 2007; Min et al., 2011; Hirsch & Archfield, 2015). Work detailed in Kotz et al. (2022) has recently identified that increases in extreme rainfall reduce economic growth rates. A study by Pendergrass and Knutti (2018) investigated the uneven nature of precipitation, finding that half the annual precipitation occurs during the wettest 12 days of the year. When assessing output from CMIP5 climate models, they also found a shortening of the average number of days needed to reach half the annual precipitation highlighting the increased importance of extreme events.

Extra-tropical cyclones (hereafter referred to as cyclones) are key components of the atmospheric general circulation due to their ability to transport large quantities of heat, moisture, and momentum. Cyclones are an important contributor to extreme weather events as their passage is associated with strong winds, precipitation, and temperature changes (Papritz et al., 2014). Studies quantifying cyclone-associated precipitation find that up to 90% of precipitation in the mid-latitude storm tracks is associated with frontal systems and their associated cyclones (Catto et al., 2012; Hawcroft et al., 2012; Utsumi et al., 2017). Pfahl and Wernli (2012) has also identified that a high percentage of precipitation extremes are directly related to cyclones, with some locations having up to 80% of their precipitation extremes associated with cyclones. Utsumi et al. (2017) also identify that large amounts of extreme precipitation in mid-latitude regions are associated with cyclones. McErlich, McDonald, Schuddeboom, et al. (2023) has also recently demonstrated that larger precipitation extremes are associated with regions where large scale precipitation processes, such as cyclones, dominate.

In this study we use a regionally dependent precipitation threshold to classify precipitation extremes relative to the cyclone centre. Cyclone composites for both average and extreme precipitation are calculated from the ERA5 reanalysis. Composites are then partitioned into different stages of the lifecycle to assess the spatial and temporal evolution of extremes. The rate at which extremes precipitation changes throughout the cyclone lifecycle is then quantified.

2 Datasets and Methods

2.1 ERA5

We use output from the ERA5 reanalysis to identify cyclones over the Southern Hemisphere for the years 1980 - 2019 inclusive. ERA5 is available on a 0.25° latitude/longitude grid and at an hourly temporal resolution, however three hourly data was used in this study. Previous work (McDonald & Cairns, 2020; McErlich, McDonald, Schuddeboom, et al., 2023; McErlich, McDonald, Renwick, & Schuddeboom, 2023) shows that ERA5 is consistent with a number of satellite and reanalysis datasets for determining precipitation. This past research also shows that ERA5 can be used to successfully examine cyclonic structure within a compositing framework for 10m wind speeds, total column water vapour, cloud liquid water, and precipitation.

2.2 Cyclone tracking and compositing methodology

Work by Crawford and Serreze (2016) introduces and details the mean sea level pressure (MSLP) based cyclone tracking algorithm used in this study. Previous work in McErlich, McDonald, Renwick, and Schuddeboom (2023) also describes application of the cyclone tracking algorithm over the Southern Hemisphere using ERA5, but a short summary is included in the following paragraphs.

Local minima in the ERA5 mean sea level pressure (MSLP) field are used to identity cyclone centres. This covers the time period between 1980 - 2019 with a temporal resolution of three hour and cyclones are identified using local minima in the MSLP field. A radius-based threshold is also used to identify whether it is a closed low pressure system, and thus can be characterised as a cyclone. A maximum propagation speed of 150 kmhr^{-1} is used to join related low pressure centres into continuous cyclone tracks. Criteria are also applied to reject systems that have a lifespan shorter than 24 hours, a track length less than 100km, or do not spend some part of their lifetime at latitudes south of 30°S. This causes cyclone tracks to predominately be concentrated over the Southern Ocean (not shown; see Figure 1 McErlich, McDonald, Renwick, & Schuddeboom, 2023); This is in agreement with previous research that analyzed Southern hemisphere cyclone tracks (e.g. Hoskins & Hodges, 2005; Bengtsson et al., 2006; Hodges et al., 2011).

The identified cyclone centers are then used to transform ERA5 data into a cyclone centered-coordinate system in the form of cyclone composites as detailed in McErlich, McDonald, Renwick, and Schuddeboom (2023). Cyclone composites are calculated using a radius of 2000 km, which is commonly used in previous work (e.g. Field & Wood, 2007; Field et al., 2008; Naud et al., 2012; Booth et al., 2018; McErlich, McDonald, Renwick, & Schuddeboom, 2023). Individual composites are rotated so that the direction of propagation of the cyclone is chosen to be travelling eastward. Given the zonal westerly winds over the Southern Ocean many cyclones require little rotation. This step approximately aligns the position of the warm/cold fronts and the area of warm, moist air associated with them. While not all fronts will be at the same position relative to the direction of the cyclone, this rotation acts to focus the structure of the composite (Govekar et al., 2011).

2.3 Analysis of cyclone lifecycle

To better understand changes in precipitation as the cyclone evolves, we partition the cyclones into three distinct developmental phases. We classify cyclones relative to the time of their maximum depth, which is defined as the time of maximum difference between the edge pressure and central pressure of the cyclone. We define three phases to represent periods of deepening, peak intensity and decay within the cyclone. The phase of peak intensity is defined as 6 hours either side of the time of maximum depth. The deepening phase is defined as measurements between 6 hours and 18 hours previous to the time of maximum depth. The decay phase is defined as measurements between 6 and 18 hours after the time of maximum depth.

In order to partition the cyclones into phases of deepening, peak intensity, and decay, a further criterion based on the deepening rate ($\frac{\partial p}{\partial t}$, scaled by latitude) was also assessed. Cyclone tracks were kept if the deepening rate changed from positive (indicating strengthening) during the deepening phase to negative (indicating weakening) during the decay phase. Cyclone track that pass this criterion are masked to only include data within the previously defined cyclone phases. Tracks without measurements 18 hours before and after the point of peak intensity are rejected, causing a minimum cyclone lifespan of 36 hours within the subset of cyclone tracks used in this analysis.

2.4 Identification of cyclone extremes associated with cyclones

In order to identify regions of the cyclone that correspond to precipitation extremes, we use a methodology introduced in McErlich, McDonald, Schuddeboom, et al. (2023). This produces regionally dependent thresholds for extreme precipitation which are then applied to a cyclone compositing framework. Firstly, a spatial map of precipitation wet day frequency is produced using a 1 mm/day threshold to define a wet day over the Southern hemisphere. This threshold is commonly used within the community (Polade et al., 2014; Schär et al., 2016) and is also used in a number of extreme precipitation indices as defined by the Expert Team on Climate Change Detection and Indices (ETCCDI; Zhang et al., 2011).

Secondly, rainfall data from regions of the same precipitation frequency are grouped together; This data is then aggregated to produce cumulative precipitation intensity distributions. McErlich, McDonald, Schuddeboom, et al. (2023) establishes this methodology forms coherent precipitation groupings, even through it connects spatially disparate regions together. The variability within wet day frequency regions has also been shown to be comparable to that within geographic regions.

Precipitation around the cyclone composite is then assessed to determine if it is an extreme for a given latitude/longitude based on the corresponding wet day frequency. Wet day frequency regions are identified within the cyclone composites using the geographic position of the cyclone centres, as determined by the tracking algorithm. A spatially dependent threshold for precipitation extremes defined by the locations wet day frequency is then applied to the cyclone composites, removing data below the nth percentile value of the aggregated precipitation. This process is repeated across each wet day frequency region to account for changes in the underlying processes that generate precipitation. This methodology produces masked cyclone composites consisting of only precipitation at locations where it is above the spatially dependent nth percentile threshold.

Setting this threshold to the upper tail of the precipitation distribution determines cyclone composites for the extremes. Here we assess both the 90th and the 98th percentiles allowing us to examine precipitation extremes. We also mask precipitation by a 1 mm per day wet day threshold (Zhang et al., 2011) and 50th percentile value. While not indicative of extremes, these sets of composites provide data which the extreme composites can be compared with, allowing us to understand unique features associated with extreme precipitation. We note that the wet day frequency has a narrower range (see Figure 1 McErlich, McDonald, Schuddeboom, et al., 2023) over the Southern Ocean where the concentration of cyclones is the highest. This means there will be less variability in the extreme precipitation thresholds over the Southern Ocean than for a global analysis.

3 Results

Figure 1 shows the occurrence of precipitation for the wet day precipitation, 50th, 90th and 98th percentile masked composites in the cyclone centered coordinate system. Here precipitation occurrence is defined within each masked subset of composites as the percentage of time precipitation is identified. To highlight the changes in the structure, each set of composites are shown on different colour scales. Because of the rotation applied to the cyclone composites, the top of the composites may not align with north, so cardinal directions are not used to describe cyclone features.

Figure 1a-c shows the precipitation occurrence for the wet day precipitation during the deepening phase, with rates up to 100% relative to the cyclone. Occurrence then decreases slightly throughout the cyclone lifecycle. Given the potential for significant diabatic heating/latent heat release during the deepening phase (Wernli et al., 2002; Ludwig et al., 2014; Binder et al., 2016; Messmer & Simmonds, 2021) this pattern is expected. The spatial structure shows high precipitation occurrence about the cyclone centre, that extends in a tail towards the left side of the composite. This tail rotates clockwise throughout the lifecycle, likely highlighting the warm seclusion identified in idealised models.

Looking at the 50th percentile masked composites, Figure 1d-f similarly shows highest precipitation occurrence during the deepening phase, of up to 80%, before decreasing in later lifecycle stages. The spatial region associated with high occurrences shows a reduced extent from that seen in 1a-c, with a more pronounced comma structure in the upper left quadrant of the cyclone. This comma structure in precipitation has long been identified in conceptual models of cyclones (see Semple, 2003) and is likely related to the warm conveyor belt. This comma rotates clockwise as the cyclone evolves and the drier poleward area of the cyclone moves equatorward towards the cyclone centre.

Comparable patterns are observed when looking at the 90th percentile masked cyclone composites for extreme precipitation occurrence (Figure 1g-i) and the 98th percentile masked composites (Figure 1j-l). Precipitation occurrence is once again greatest during deepening, before decreasing in the peak intensity and decay phases. The structure of the high occurrence comma also rotates clockwise through the cyclone lifecycle. A further reduction in the spatial extent of high occurrence regions from Figure 1d-f is observed, such that the occurrence of precipitating extremes outside the comma is very

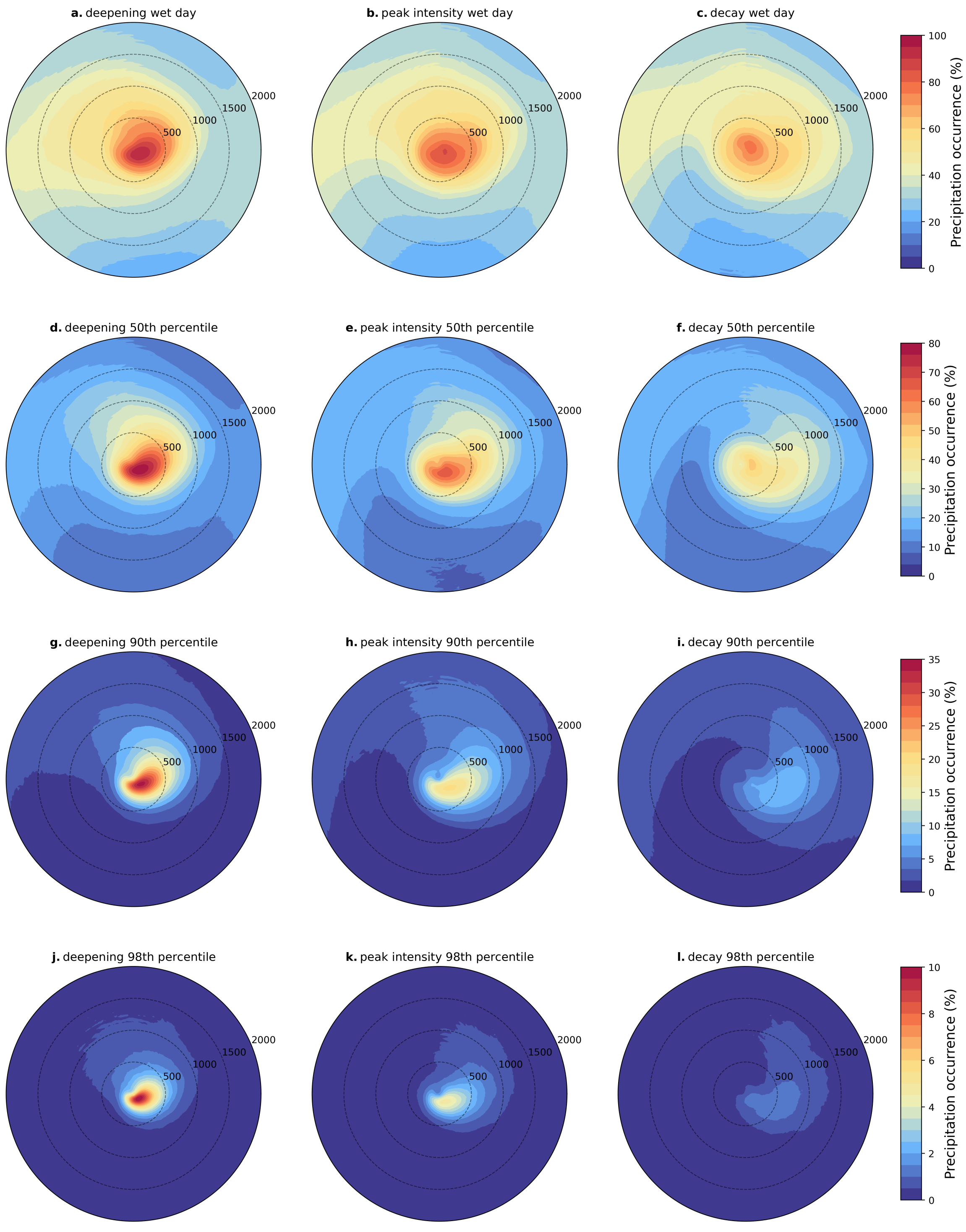

Figure 1. ERA5 cyclone composites of precipitation occurrence between 1980 - 2019 broken into the deepening, peak intensity and decay phases for (a - c) wet day precipitation (d - f) precipitation masked by the 50th percentile value (g - i) precipitation masked by the 90th percentile value (k - l) precipitation masked by the 98th percentile value.

low. For the 90th percentile masked composites precipitation extremes rarely occur within the drier poleward region of the cyclone; For the 98th percentile masked composites precipitation extremes rarely occur outside of the comma structure.

To examine extreme precipitation from a different perspective, the fraction of the total precipitation fraction associated with each threshold is derived in Figure 2. This fraction is defined as the ratio of precipitation accumulated above a given threshold and the total accumulated precipitation (Supplementary Figure 1). For the wet day percentiles, this accumulation is determined using a 1 mm per day threshold. The nth percentile threshold is used for the 50th, 90th and 98th percentile masked cyclone composites. Figure 2 shows precipitation fraction calculated for each point across the cyclone composite, for the wet day precipitation and 50th, 90th and 98th percentile masked composites. Note the different colour scales on each row of subplots used to distinguish structure.

Figure 2a-c shows areas within the cyclone composites where almost 100% of precipitation is above the 1 mm wet day threshold. Higher precipitation fraction is concentrated in the comma region of the cyclone composite and in the warm equatorward region of the cyclone. Precipitation fraction is greatest during the deepening phase, decreases and rotates clockwise in the peak intensity phase, then weakens during the decay phase. The area of lowest precipitation fraction occurs in the cold poleward region of the composite, where more of the rainfall is below the 1 mm wet day threshold suggesting a region dominated by drizzle. This region moves equatorward up the left flank of the cyclone into the upper left quadrant as the cyclone evolves. An almost identical pattern is seen for the 50th percentiles masked composites on Figure 2d-f. Differences include a lesser precipitation fraction, and a reduced spatial extent similar to that seen between Figure 1a-c and d-f.

When looking at the precipitation fraction for the 90th percentile masked composites, Figure 2g-i shows a decrease compared to the 50th percentile threshold as would be expected. The fraction of the total precipitation linked to events above this threshold are still highest during the deepening phase, but the greatest precipitation fraction (almost 80%) is lower compared to Figure 2a/d. That up to 80% of precipitation is associated with the top 10% of the precipitation distribution is meaningful, and highlights the importance of cyclones for extreme precipitation in general. Regions of high precipitation fraction are more concentrated in the centre of the cyclone compared to Figure 2a-f, but with a broad region of 40% to 50% precipitation fraction within the equatorward region of the cyclone highlighting the importance of extreme precipitation in the overall accumulation. A clockwise rotation in regions of highest precipitation fraction is also observed throughout the cyclone evolution, as the precipitation fraction weakens throughout the peak intensity and decay phases.

When applying the strictest threshold and masking by the 98th percentile value, Figure 2j-l shows a further decrease in the fraction of the total precipitation associated with events above this threshold. Though, the greatest precipitation fraction is close to 50% and occurs during the deepening phase, before a reduction and clockwise rotation is seen similar to Figure 2g-i. Structurally the large precipitation fraction shows the smallest extent at the 98th percentile, being most concentrated within the comma region of near the cyclone centre.

Results observed for the precipitation occurrence and fraction show similarities in structure between the masked cyclone composites. Figure 3a-b shows the Pearson correlation coefficients and spatial averages for the precipitation fraction across the cyclone composite as shown on Figures 1 and 2. Correlation is calculated pairwise between each set of cyclone composites, spatially across the composite. Results also show that precipitation is greatest during the deepening phase, and then weakens as the cyclone evolves. However, Figures 1 - 2 show this weakening happens at different rates. To investigate the similarities between the cyclone composites and to quantify this weakening, the ra-

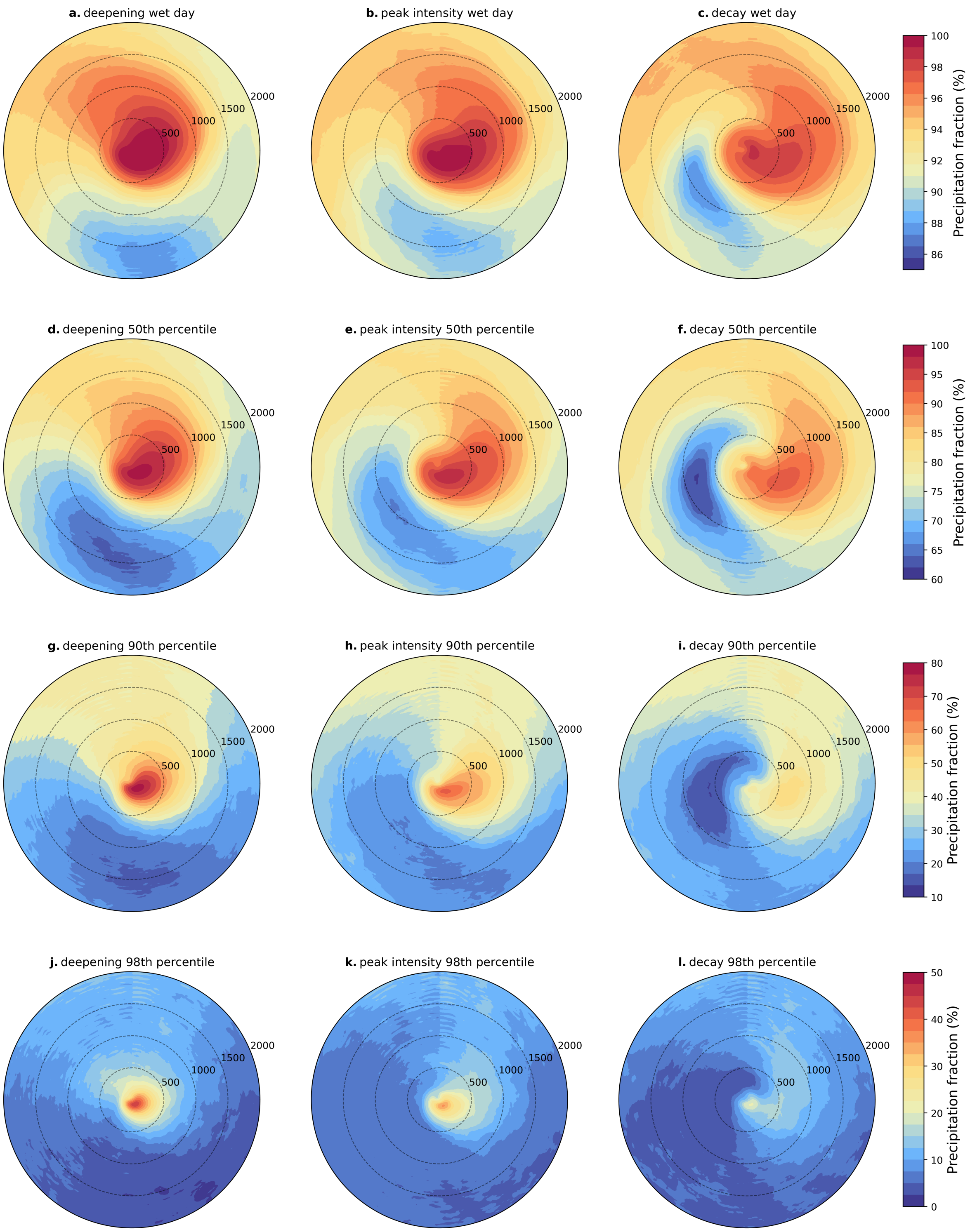

Figure 2. ERA5 cyclone composites of precipitation fraction between 1980 - 2019 broken into the deepening, peak intensity and decay phases for (a - c) wet day precipitation (d - f) precipitation masked by the 50th percentile value (g - i) precipitation masked by the 90th percentile value (k - l) precipitation masked by the 98th percentile value.

tio of the averages in the peak intensity and decay phases relative to the deepening phase are also shown in Figure 3c-d.

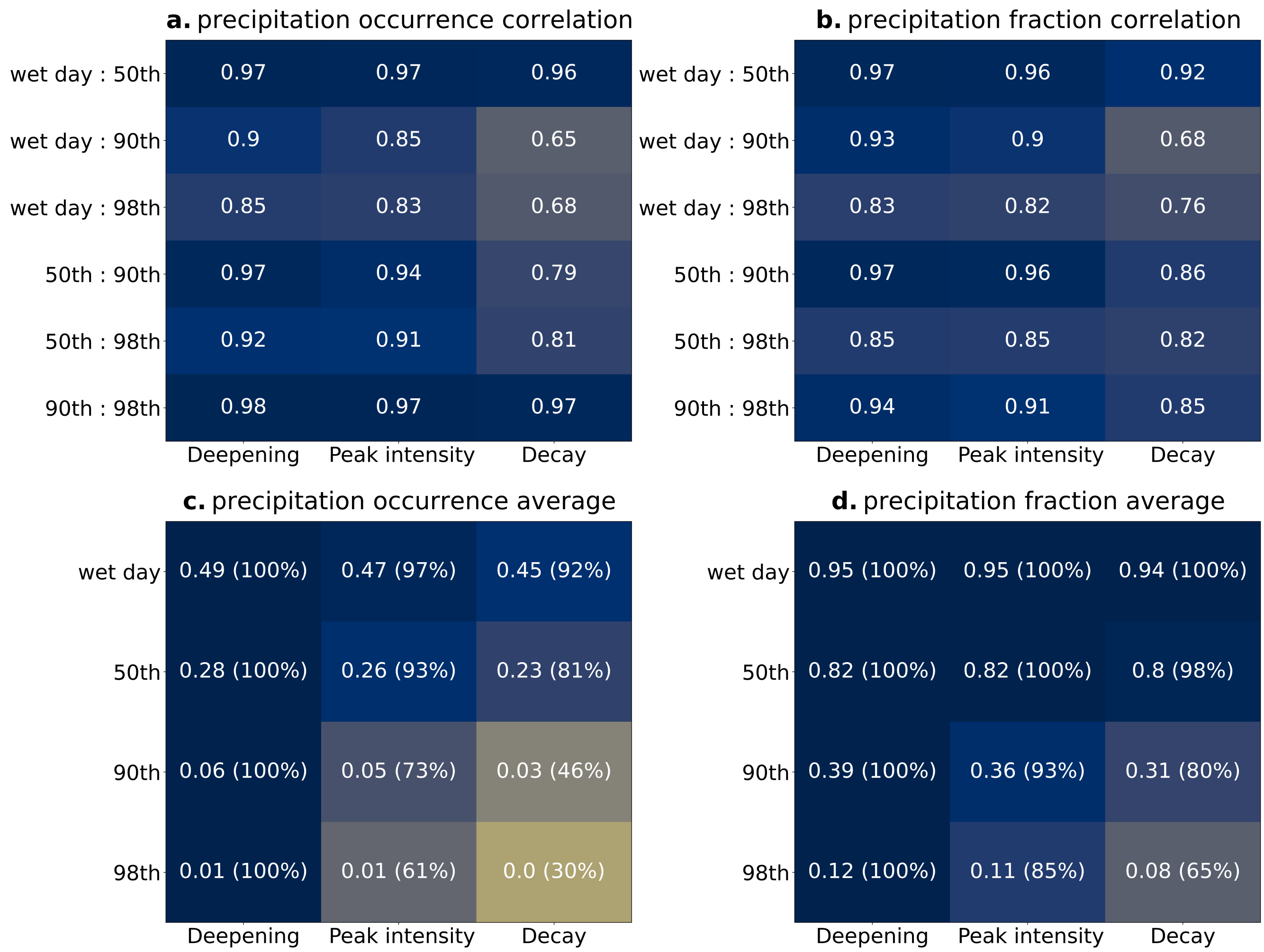

Figure 3. a) Pairwise Pearson correlation coefficients for cyclone composites within the deepening, peak intensity and decay phases for the precipitation occurrence b) same as a) but for precipitation fraction c) Precipitation averages across the cyclone composites within the deepening, peak intensity and decay phases for the precipitation occurrence d) same as c) but for precipitation fraction. The bracketed percentages for (c - d) indicate precipitation averages as a proportion of the corresponding deepening phase value.

Pairwise spatial correlations for the precipitation occurrence (Figure 3a) show strong agreement between each masked composites at the same period in the cyclone lifecycle. Correlation is strongest during the deepening phase in all cases. Correlation is lowest between the wet day precipitation and 90/98th percentile masked composites, but still strong within the deepening phase. When comparing the wet day precipitation/50th percentiles and 90th/98th masked composites, the spatial correlation remains consistently high across the cyclone lifecycle. When looking at the precipitation fraction, the pairwise correlation shows a similar trend to that observed for the precipitation occurrence. There is a strong correlation during the deepening phase and weaker correlation during the decay phase.

Looking at the average precipitation occurrence across the cyclone (Figure 3c), not only do the extremes have lower occurrence that the non-extreme precipitation, but drop off significantly faster. The wet day precipitation and 50th percentile masked composites decrease to 90% and 81% of the deepening value during the decay phase, respectively. The 90th percentile composites decrease to 46% of the deepening value and the 98th percentile composites to 30% of the deepening value during the decay phase. This indicates as you increase the threshold for determining extremes, they will be disproportionately be experienced most often during the deepening phase, as the occurrence weakens greatly by the decay phase. Averages for the precipitation fraction (Figure 3d) display a similar trend. The 90th and 98th percentile masked composites decrease to 80% and 65% of the deepening value, respectively, while the wet day precipitation and 50th percentile masked composites decrease negligibly. This highlights that as you increase the threshold for the extremes the deepening phase becomes more important, as a lower proportion of the total precipitation experienced in future cyclone phases can be defined as extreme.

4 Discussion and Conclusion

Using a spatially dependent threshold for precipitation, we have developed a simple methodology to assess the contribution to accumulation and the occurrence of precipitation extremes by masking data within a cyclone compositing framework. This methodology is based on grouping regions of similar precipitation frequency together, which have been shown to be influenced by the same underlying dynamic and thermodynamic precipitation processes (McErlich, McDonald, Schuddeboom, et al., 2023). While some past studies investigate precipitation extremes and how they connect to cyclones (e.g. Pfahl & Wernli, 2012; Catto & Dowdy, 2021; Messmer & Simmonds, 2021), this is the first investigation from a cyclone centered perspective over the Southern Hemisphere, instead of focusing on assessing the spatial distributions of cyclones.

Here we see that the greatest precipitation occurrence and fraction of total precipitation occur before the cyclone reaches its peak intensity. The precipitation accumulation (Supplementary Figure 1) is also greatest during the deepening phase, meaning precipitation extremes will be experienced most acutely during the deepening phase. This is not a new result, as Booth et al. (2018) and McErlich, McDonald, Renwick, and Schuddeboom (2023) also show that greater precipitation occurs before the cyclone reaches peak intensity. These studies also show a weakening in the comma structure of precipitation through the cyclone lifecycle. However, we show that extreme precipitation also displays a similar trend. For both the 90th and 98th masked percentile composites, the precipitation occurrence and fraction is greatest during the deepening phase and then decays slightly as the cyclone evolves. Many studies have shown support for the concept that the release of latent heating associated with precipitation leads to the intensification of a cyclone (Wernli et al., 2002; Ludwig et al., 2014; Binder et al., 2016; Messmer & Simmonds, 2021), which is consistent with our findings.

Figure 3c-d shows that precipitation occurrence and precipitation fraction weakens at a faster rate as you increase from the 90th to 98th percentile of precipitation. This suggests a larger diabatic heating and subsequent intensification of the cyclone from extreme precipitation events. Figure 3c-d also shows that the precipitation occurrence shows a larger change from the deepening to the decay phase than the precipitation fraction at every extreme threshold. This suggests that during the decay phase a larger amount of rainfall is associated with a smaller number of extreme events.

Looking at the spatial pattern of precipitation within cyclone composites, Figures 1 and 2 show that as you apply a stricter threshold to mask precipitation there is a reduction in the spatial extent of both high precipitation occurrence and fraction. As you move towards the extremes, precipitation is more concentrated towards the centre of the cyclone within the comma region linked to the warm conveyor belt.

Figure 3a-b shows that for the precipitation occurrence and fraction, the 90th and 98th percentile masked composites show strong spatial correlation across all states of the cyclone lifecycle. The wet day precipitation and 50th and 90th/98th percentile masked cyclone composites shows strong agreement for precipitation occurrence and fraction during the deepening and peak intensity phases, but weaker agreement during the decay phase. These correlations show that the spatial regions of the cyclone where precipitation extremes are important remain similar across the cyclone lifecycle, suggesting that knowing the median precipitation pattern could provide insight into the upper tail of the distributions, at least for the precipitation occurrence and fraction.

This work has determined the spatial structure of extreme precipitation relative to cyclone centres, and provided a quantification of how these extremes change as the cyclone evolves. However, the underlying processes that determine precipitation have not been assessed to provide a physical justification for results seen in this work. McErlich, McDonald, Schuddeboom, et al. (2023) has shown that vertical velocity and convective available potential energy are important drivers of global precipitation and that precipitation is determined, in part, by the occurrence of these precipitation-generating processes. Future work will examine these processes to determine how they influence the behaviour of precipitation and precipitation extremes in cyclones through their lifecycle.

Acknowledgments

The ERA5 reanalysis products were obtained from the Copernicus Climate Data Store (https://cds.climate.copernicus.eu/). Data used to visualise the figures is available at https://zenodo.org/record/7787119. We would also like to acknowledge funding from the Ministry of Business, Innovation and Employment (MBIE), New Zealand, through the Whakahura project (grant number E7141).

References

Bell, J. E., Brown, C. L., Conlon, K., Herring, S., Kunkel, K. E., Lawrimore, J., ... Uejio, C. (2018). Changes in extreme events and the potential impacts on human health. *Journal of the Air & Waste Management Association*, *68*(4), 265-287. doi: 10.1080/10962247.2017.1401017

Bengtsson, L., Hodges, K. I., & Roeckner, E. (2006). Storm tracks and climate change. *Journal of Climate*, *19*(15), 3518 - 3543. Retrieved from `https://journals.ametsoc.org/view/journals/clim/19/15/jcli3815.1.xml` doi: 10.1175/JCLI3815.1

Binder, H., Boettcher, M., Joos, H., & Wernli, H. (2016). The role of warm conveyor belts for the intensification of extratropical cyclones in northern hemisphere winter. *Journal of the Atmospheric Sciences*, *73*(10), 3997 - 4020. doi: 10.1175/JAS-D-15-0302.1

Booth, J. F., Naud, C. M., & Jeyaratnam, J. (2018). Extratropical cyclone precipitation life cycles: A satellite-based analysis. *Geophysical Research Letters*, *45*(16), 8647-8654. Retrieved from `https://agupubs.onlinelibrary.wiley.com/doi/abs/10.1029/2018GL078977` doi: https://doi.org/10.1029/2018GL078977

Catto, J. L., & Dowdy, A. (2021). Understanding compound hazards from a weather system perspective. *Weather and Climate Extremes*, *32*, 100313. Retrieved from `https://www.sciencedirect.com/science/article/pii/S2212094721000116` doi: https://doi.org/10.1016/j.wace.2021.100313

Catto, J. L., Jakob, C., Berry, G., & Nicholls, N. (2012). Relating global precipitation to atmospheric fronts. *Geophysical Research Letters*, *39*(10). doi: https://doi.org/10.1029/2012GL051736

Crawford, A. D., & Serreze, M. C. (2016). Does the summer arctic frontal zone influence arctic ocean cyclone activity? *Journal of Climate*, *29*(13), 4977 - 4993. doi: 10.1175/JCLI-D-15-0755.1

Field, P. R., Gettelman, A., Neale, R. B., Wood, R., Rasch, P. J., & Morrison, H. (2008). Midlatitude cyclone compositing to constrain climate model behavior using satellite observations. *Journal of Climate*, *21*(22), 5887 - 5903. doi: 10.1175/2008JCLI2235.1

Field, P. R., & Wood, R. (2007). Precipitation and cloud structure in midlatitude cyclones. *Journal of Climate*, *20*(2), 233 - 254. doi: 10.1175/JCLI3998.1

Govekar, P. D., Jakob, C., Reeder, M. J., & Haynes, J. (2011). The three-dimensional distribution of clouds around southern hemisphere extratropical cyclones. *Geophysical Research Letters*, *38*(21). doi: https://doi.org/10.1029/2011GL049091

Hawcroft, M., Shaffrey, L., Hodges, K., & Dacre, H. (2012, 12). How much northern hemisphere precipitation is associated with extratropical cyclones? *Geophysical Research Letters*, *39*, 24809-. doi: 10.1029/2012GL053866

Hirsch, R. M., & Archfield, S. A. (2015, Mar 01). Not higher but more often. *Nature Climate Change*, *5*(3), 198-199. doi: 10.1038/nclimate2551

Hodges, K. I., Lee, R. W., & Bengtsson, L. (2011). A comparison of extratropical cyclones in recent reanalyses era-interim, nasa merra, ncep cfsr, and jra-25. *Journal of Climate*, *24*(18), 4888 - 4906. Retrieved from `https://journals.ametsoc.org/view/journals/clim/24/18/2011jcli4097.1.xml` doi: 10.1175/2011JCLI4097.1

Hoskins, B. J., & Hodges, K. I. (2005). A new perspective on southern hemisphere storm tracks. *Journal of Climate*, *18*(20), 4108 - 4129. doi: 10.1175/JCLI3570.1

Howe, P. D., Boudet, H., Leiserowitz, A., & Maibach, E. W. (2014, Nov 01). Mapping the shadow of experience of extreme weather events. *Climatic Change*, *127*(2), 381-389. doi: 10.1007/s10584-014-1253-6

Jahn, M. (2015). Economics of extreme weather events: Terminology and regional impact models. *Weather and Climate Extremes*, *10*, 29-39. doi: https://doi.org/10.1016/j.wace.2015.08.005

Konapala, G., Mishra, A. K., Wada, Y., & Mann, M. E. (2020). Climate change will affect global water availability through compounding changes in seasonal precipitation and evaporation [Journal Article]. *Nature Communications*, *11*(1), 3044. doi: 10.1038/s41467-020-16757-w

Kotz, M., Levermann, A., & Wenz, L. (2022, Jan 01). The effect of rainfall changes on economic production. *Nature*, *601*(7892), 223-227. doi: 10.1038/s41586-021-04283-8

Ludwig, P., Pinto, J. G., Reyers, M., & Gray, S. L. (2014). The role of anomalous sst and surface fluxes over the southeastern north atlantic in the explosive development of windstorm xynthia. *Quarterly Journal of the Royal Meteorological Society*, *140*(682), 1729-1741. doi: https://doi.org/10.1002/qj.2253

McDonald, A. J., & Cairns, L. H. (2020). A new method to evaluate reanalyses using synoptic patterns: An example application in the ross sea/ross ice shelf region. *Earth and Space Science*, *7*(1), e2019EA000794. Retrieved from `https://agupubs.onlinelibrary.wiley.com/doi/abs/10.1029/2019EA000794` doi: https://doi.org/10.1029/2019EA000794

McErlich, C., McDonald, A., Renwick, J., & Schuddeboom, A. (2023). An assessment of southern hemisphere extra-tropical cyclones in era5 using windsat. *Authorea Preprints*. doi: 10.22541/essoar.167591115.54167961/v1

McErlich, C., McDonald, A., Schuddeboom, A., Vishwanathan, G., Renwick, J., & Rana, S. (2023). Positive correlation between wet day frequency and intensity

linked to universal precipitation drivers. *Nature Geosience*.
Messmer, M., & Simmonds, I. (2021). Global analysis of cyclone-induced compound precipitation and wind extreme events. *Weather and Climate Extremes*, *32*, 100324. doi: https://doi.org/10.1016/j.wace.2021.100324
Min, S.-K., Zhang, X., Zwiers, F. W., & Hegerl, G. C. (2011, Feb 01). Human contribution to more-intense precipitation extremes. *Nature*, *470*(7334), 378-381. doi: 10.1038/nature09763
Morss, R. E., Wilhelmi, O. V., Meehl, G. A., & Dilling, L. (2011). Improving societal outcomes of extreme weather in a changing climate: an integrated perspective. *Annual Review of Environment and Resources*, *36*, 1–25.
Naud, C. M., Posselt, D. J., & van den Heever, S. C. (2012). Observational analysis of cloud and precipitation in midlatitude cyclones: Northern versus southern hemisphere warm fronts. *Journal of Climate*, *25*(14), 5135 - 5151. doi: 10.1175/JCLI-D-11-00569.1
Papritz, L., Pfahl, S., Rudeva, I., Simmonds, I., Sodemann, H., & Wernli, H. (2014). The role of extratropical cyclones and fronts for southern ocean freshwater fluxes. *Journal of Climate*, *27*(16), 6205 - 6224. doi: 10.1175/JCLI-D-13-00409.1
Pendergrass, A. G., & Knutti, R. (2018). The uneven nature of daily precipitation and its change. *Geophysical Research Letters*, *45*(21), 11,980-11,988. Retrieved from `https://agupubs.onlinelibrary.wiley.com/doi/abs/10.1029/2018GL080298` doi: https://doi.org/10.1029/2018GL080298
Pfahl, S., & Wernli, H. (2012). Quantifying the relevance of cyclones for precipitation extremes. *Journal of Climate*, *25*(19), 6770 - 6780. doi: 10.1175/JCLI-D-11-00705.1
Polade, S. D., Pierce, D. W., Cayan, D. R., Gershunov, A., & Dettinger, M. D. (2014, Mar 13). The key role of dry days in changing regional climate and precipitation regimes. *Scientific Reports*, *4*(1), 4364. doi: 10.1038/srep04364
Schär, C., Ban, N., Fischer, E. M., Rajczak, J., Schmidli, J., Frei, C., ... Zwiers, F. W. (2016, Jul 01). Percentile indices for assessing changes in heavy precipitation events. *Climatic Change*, *137*(1), 201-216. doi: 10.1007/s10584-016-1669-2
Seddon, A. W. R., Macias-Fauria, M., Long, P. R., Benz, D., & Willis, K. J. (2016, Mar 01). Sensitivity of global terrestrial ecosystems to climate variability. *Nature*, *531*(7593), 229-232. doi: 10.1038/nature16986
Semple, A. (2003). A review and unification of conceptual models of cyclogenesis. *Meteorological Applications*, *10*, 39-59.
Seneviratne, S., Nicholls, N., Easterling, D., Goodess, C., S. Kanae, J. K., Luo, Y., ... Zhang, X. (2012). *Changes in climate extremes and their impacts on the natural physical environment* (C. Field et al., Eds.). Cambridge, UK, and New York, NY, USA: Cambridge University Press.
Seneviratne, S., Zhang, X., Adnan, M., Badi, W., Dereczynsk, C., Luca, A. D., ... Zhou, B. (2021). *Weather and Climate Extreme Events in a Changing Climate* (V. Masson-Delmotte et al., Eds.). Cambridge, UK, and New York, NY, USA: Cambridge University Press.
Utsumi, N., Kim, H., Kanae, S., & Oki, T. (2017). Relative contributions of weather systems to mean and extreme global precipitation. *Journal of Geophysical Research: Atmospheres*, *122*(1), 152-167. doi: https://doi.org/10.1002/2016JD025222
Wernli, H., Dirren, S., Liniger, M. A., & Zillig, M. (2002). Dynamical aspects of the life cycle of the winter storm 'lothar' (24–26 december 1999). *Quarterly Journal of the Royal Meteorological Society*, *128*(580), 405-429. doi: https://doi.org/10.1256/003590002321042036
Zhang, X., Alexander, L., Hegerl, G. C., Jones, P., Tank, A. K., Peterson, T. C., ... Zwiers, F. W. (2011). Indices for monitoring changes in extremes based

on daily temperature and precipitation data. *WIREs Climate Change*, *2*(6), 851-870. doi: 10.1002/wcc.147

Zhang, X., Zwiers, F. W., Hegerl, G. C., Lambert, F. H., Gillett, N. P., Solomon, S., … Nozawa, T. (2007, Jul 01). Detection of human influence on twentieth-century precipitation trends. *Nature*, *448*(7152), 461-465. doi: 10.1038/nature06025

Zscheischler, J., Westra, S., van den Hurk, B. J. J. M., Seneviratne, S. I., Ward, P. J., Pitman, A., … Zhang, X. (2018, Jun 01). Future climate risk from compound events. *Nature Climate Change*, *8*(6), 469-477. doi: 10.1038/s41558-018-0156-3

precipitation_occurrence.png.

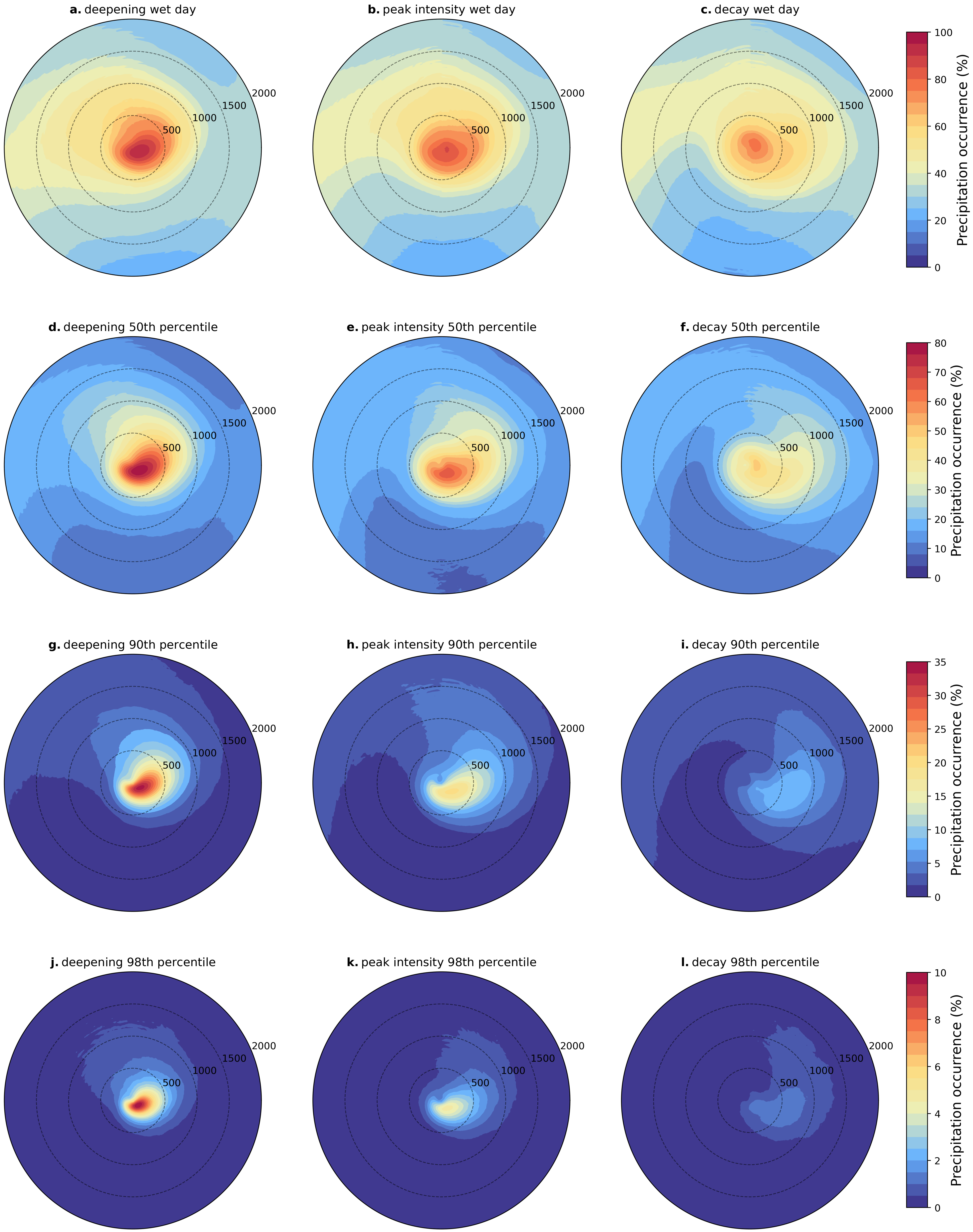
a. deepening wet day
b. peak intensity wet day
c. decay wet day
d. deepening 50th percentile
e. peak intensity 50th percentile
f. decay 50th percentile
g. deepening 90th percentile
h. peak intensity 90th percentile
i. decay 90th percentile
j. deepening 98th percentile
k. peak intensity 98th percentile
l. decay 98th percentile
500
1000
1500
2000
Precipitation occurrence (%)
0
20
40
60
80
100
0
10
20
30
40
50
60
70
80
0
5
10
15
20
25
30
35
0
2
4
6
8
10

precipitation_accumulation.png.

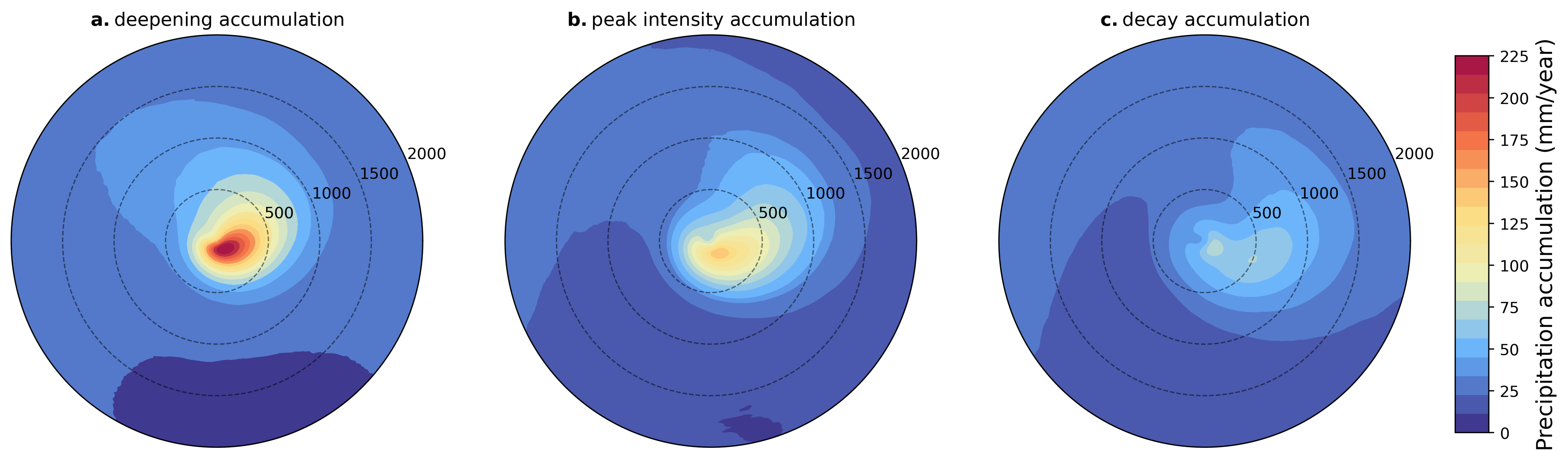
a. deepening accumulation
b. peak intensity accumulation
c. decay accumulation
500
1000
1500
2000
Precipitation accumulation (mm/year)
0
25
50
75
100
125
150
175
200
225

precipitation_fraction.png.

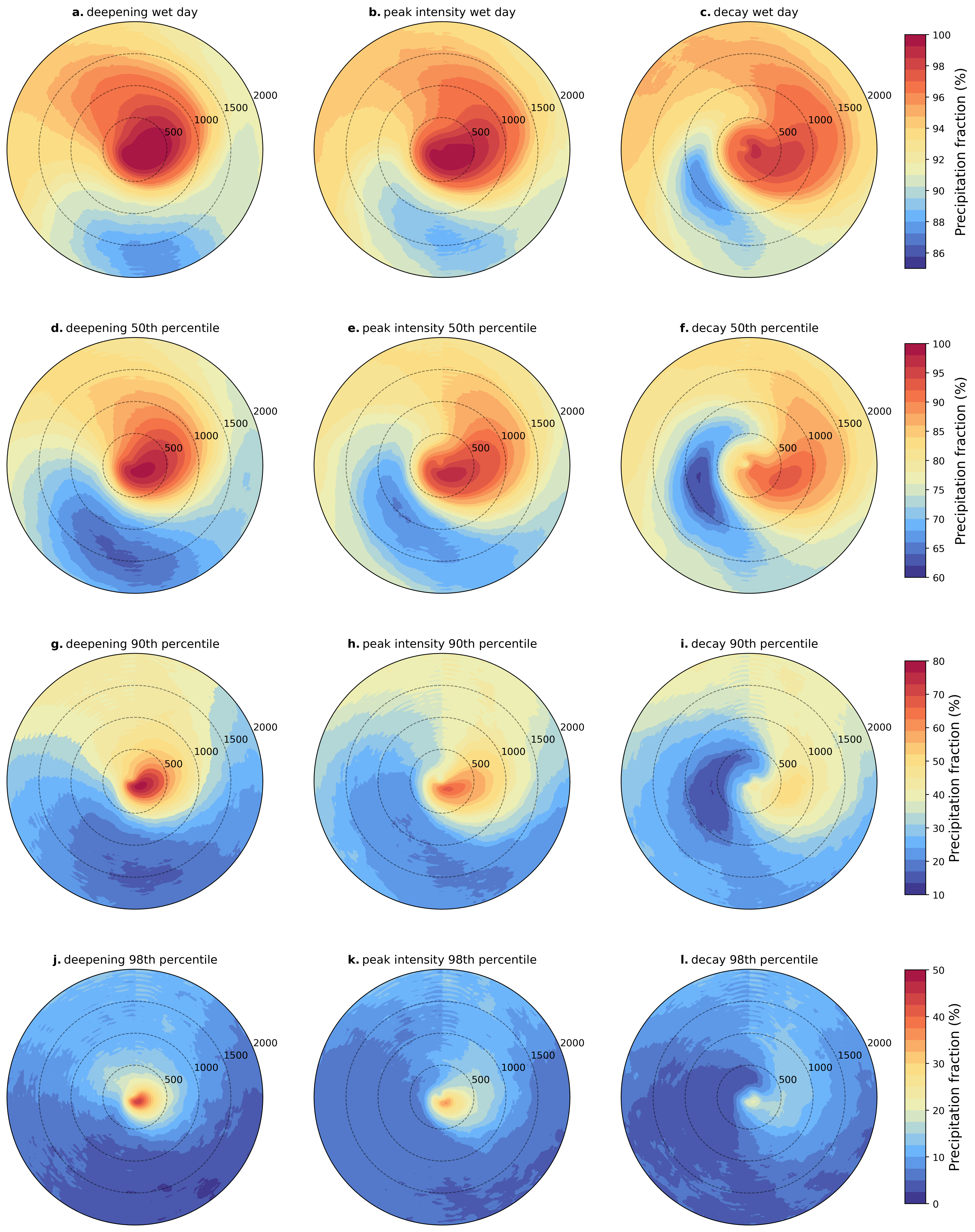

a. deepening wet day
b. peak intensity wet day
c. decay wet day
d. deepening 50th percentile
e. peak intensity 50th percentile
f. decay 50th percentile
g. deepening 90th percentile
h. peak intensity 90th percentile
i. decay 90th percentile
j. deepening 98th percentile
k. peak intensity 98th percentile
l. decay 98th percentile
500
1000
1500
2000
Precipitation fraction (%)

combined_matrix.png.

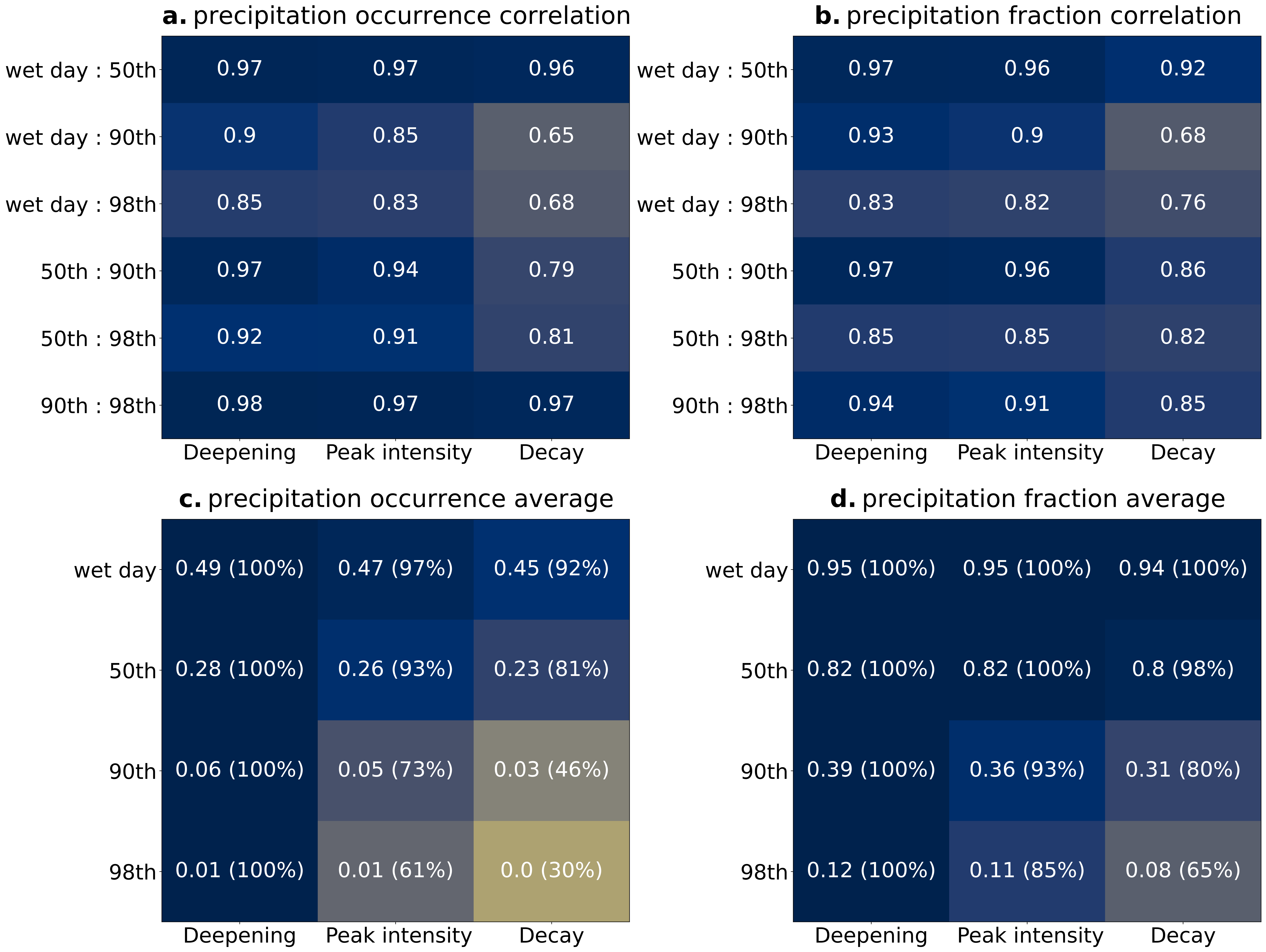
a. precipitation occurrence correlation
wet day : 50th
wet day : 90th
wet day : 98th
50th : 90th
50th : 98th
90th : 98th
0.97 0.97 0.96
0.9 0.85 0.65
0.85 0.83 0.68
0.97 0.94 0.79
0.92 0.91 0.81
0.98 0.97 0.97
Deepening
Peak intensity
Decay
b. precipitation fraction correlation
wet day : 50th
wet day : 90th
wet day : 98th
50th : 90th
50th : 98th
90th : 98th
0.97 0.96 0.92
0.93 0.9 0.68
0.83 0.82 0.76
0.97 0.96 0.86
0.85 0.85 0.82
0.94 0.91 0.85
Deepening
Peak intensity
Decay
c. precipitation occurrence average
wet day
50th
90th
98th
0.49 (100%) 0.47 (97%) 0.45 (92%)
0.28 (100%) 0.26 (93%) 0.23 (81%)
0.06 (100%) 0.05 (73%) 0.03 (46%)
0.01 (100%) 0.01 (61%) 0.0 (30%)
Deepening
Peak intensity
Decay
d. precipitation fraction average
wet day
50th
90th
98th
0.95 (100%) 0.95 (100%) 0.94 (100%)
0.82 (100%) 0.82 (100%) 0.8 (98%)
0.39 (100%) 0.36 (93%) 0.31 (80%)
0.12 (100%) 0.11 (85%) 0.08 (65%)
Deepening
Peak intensity
Decay